

Electronic Supporting Information for:

**Intrinsic Triple-Emitting 2D Copper Thiolate  
Coordination Polymer as a Ratiometric  
Thermometer Working over 400 K Range**

Oleksandra Veselska,<sup>a</sup> Darjan Podbevšek,<sup>b</sup> Gilles Ledoux,<sup>b</sup>

Alexandra Fateeva<sup>c</sup> and Aude Demessence<sup>\*a</sup>

[a] Univ Lyon, Université Claude Bernard Lyon 1, Institut de recherches sur la catalyse et l'environnement de Lyon (IRCELYON), UMR 5256 CNRS, Villeurbanne, France

[b] Univ Lyon, Université Claude Bernard Lyon 1, Institut Lumière Matière (ILM), UMR CNRS 5306, Villeurbanne, France.

[c] Univ Lyon, Université Claude Bernard Lyon 1, Laboratoire des Multimatériaux et Interfaces (LMI), UMR CNRS 5615, Villeurbanne, France.

\*aude.demessence@ircelyon.univ-lyon1.fr

*Chemical Communication*

## Experiments and methods

Routine X-ray diffraction (XRD) was carried out on a Bruker D8 Advance A25 diffractometer using Cu K $\alpha$  radiation equipped with a 1-dimensional position-sensitive detector (Bruker LynxEye). XR scattering was recorded between 4° and 90° (2 $\theta$ ) with 0.02° steps and 0.5 s per step (28 min for the scan). Divergence slit was fixed to 0.2° and the detector aperture to 189 channels (2.9°).

Single crystals of sufficient size to be measured using a laboratory diffractometer were obtained. The chosen crystal was analysed at 293(2) K using a Geminini Oxford Diffractometer (MoK $\alpha$  radiation,  $\lambda = 0.71069$  Å) equipped with a CCD camera. Reflection indexing, unit-cell parameters refinement, Lorentz-polarization correction, peak integration and background determination were carried out with the CrysAlisPro software.<sup>1</sup> An analytical absorption correction was applied using the modeled faces of the crystal.<sup>2</sup> The resulting set of hkl was used for structure solution and refinement. The structure was solved by direct methods with SIR97<sup>3</sup> and the least-square refinement on F<sup>2</sup> was achieved with the CRYSTALS software.<sup>4</sup> Non H-atoms were refined anisotropically, while H-atoms were placed geometrically and refined using the riding mode.

Crystallographic and refinements parameters are summarised in Table S2. CCDC 1570642 contains the supplementary crystallographic data for [Cu(*p*-SPhCO<sub>2</sub>Me)]<sub>n</sub>.

Thermo-gravimetric analysis (TGA) was performed with a TGA/DSC 1 STARe System from Mettler Toledo. Around 2 mg of sample was heated at a rate of 10 °C.min<sup>-1</sup>, in a 70  $\mu$ L alumina crucible, under air or nitrogen atmosphere (20 mL.min<sup>-1</sup>). A black powder corresponding to CuO was observed at the end of experiment.

The infrared spectra were obtained from a Bruker Vector 22 FT-IR spectrometer with KBr pellets at room temperature and registered from 4000 cm<sup>-1</sup> to 400 cm<sup>-1</sup>.

SEM images were obtained with FEI Quanta 250 FEG scanning electron microscope, samples were mounted on stainless pads and sputtered with Au/Pd alloy to prevent charging during observation.

UV-vis absorption spectrum was carried out with a LAMBDA 365 UV/Vis Spectrophotometer from Perkin Elmer in solid state at room temperature.

The photoluminescence measurements were performed on a homemade apparatus. The sample was illuminated by a EQ99X laser driven light source filtered by a Jobin Yvon Gemini 180 monochromator. The exit slit from the monochromator was then reimaged on the sample by two 100m focal length, 2 inch diameter MgF<sub>2</sub> lenses. The whole apparatus has been calibrated by means of a Newport 918D Low power calibrated photodiode sensor over the range 190-1000 nm. The resolution of the system being 4 nm. The emitted light from the sample is collected by an optical fiber connected to a Jobin-Yvon TRIAX320 monochromator equipped with a cooled CCD detector. At the entrance of the monochromator different long pass filter can be chosen in order to eliminate the excitation light. The resolution of the detection system is 2 nm.

**Synthesis of [Cu(*p*-SPhCO<sub>2</sub>Me)]<sub>n</sub>:** H<sub>2</sub>SO<sub>4</sub> solution (1 mL, 0.5 M) is added to a solution of CuCl<sub>2</sub>.2H<sub>2</sub>O (63 mg, 0.37 mmol) in 5 mL of DMF, then *p*-HSPHCO<sub>2</sub>Me (43 mg, 0.25 mmol) dissolved in 5 mL of DMF is introduced. The 20 mL vial is closed and the mixture is heated at 120°C for 24h. The resulting pale yellow solid is isolated by centrifuge and washed three times with DMF and three times with acetone and then dried in air. The solid is not soluble in any solvent.

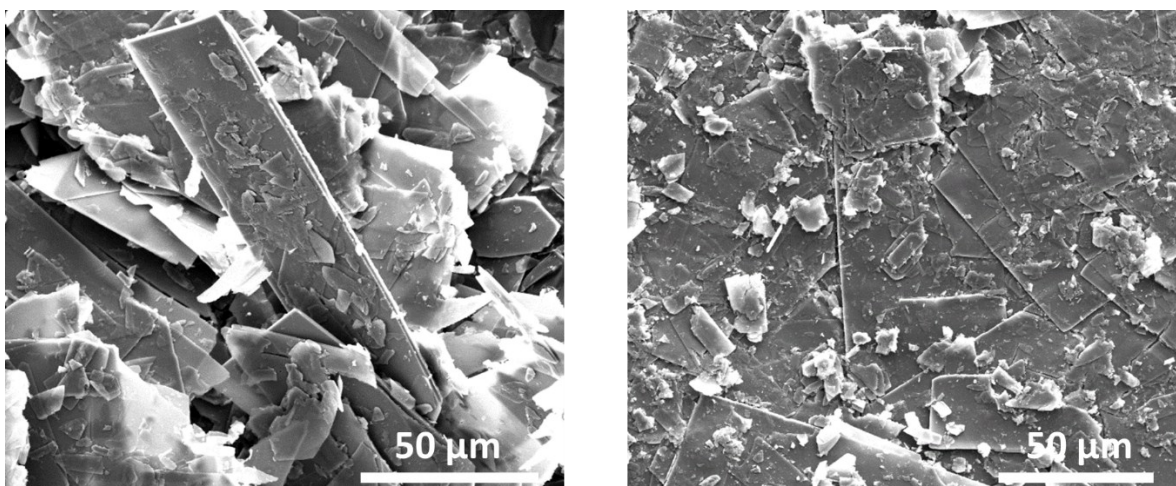


**Figure S1.** SEM images of  $[\text{Cu}(p\text{-SPhCO}_2\text{Me})]_n$ .

**Table S1.** Crystallographic data for  $[\text{Cu}(p\text{-SPhCO}_2\text{Me})]_n$ .

Empirical formula	$\text{C}_8\text{H}_7\text{Cu}_1\text{O}_2\text{S}$
$M_r$	230.75
Crystal size ( $\mu\text{m}$ )	250*50*10
Crystal system	monoclinic
Space group	$Pn$
$a$ ( $\text{\AA}$ )	3.9655(5)
$b$ ( $\text{\AA}$ )	19.103(3)
$c$ ( $\text{\AA}$ )	5.2888(9)
$\alpha$ ( $^\circ$ )	90
$\beta$ ( $^\circ$ )	93.343(14)
$\gamma$ ( $^\circ$ )	90
$V$ ( $\text{\AA}^3$ )	399.96(11)
$Z$	2
$\lambda$ ( $\text{\AA}$ )	0.71073
Number of reflections	1325
Parameters	110
$R[F^2 > 2\sigma(F^2)]$	0.0562
$wR(F^2)$	0.02356
GoF	0.95

**Table S2.** Selected distances and angles from the structure of  $[\text{Cu}(p\text{-SPhCO}_2\text{Me})]_n$ .

Cu-Cu (Å)	3.313(3)	3.493(3)	
Cu-S (Å)	2.244(3)	2.255(3)	2.282(4)
Cu-S-Cu (°)	93.8(2)	101.0(2)	123.6(2)
S-Cu-S (°)	114.0(2)	122.2(2)	123.6(2)

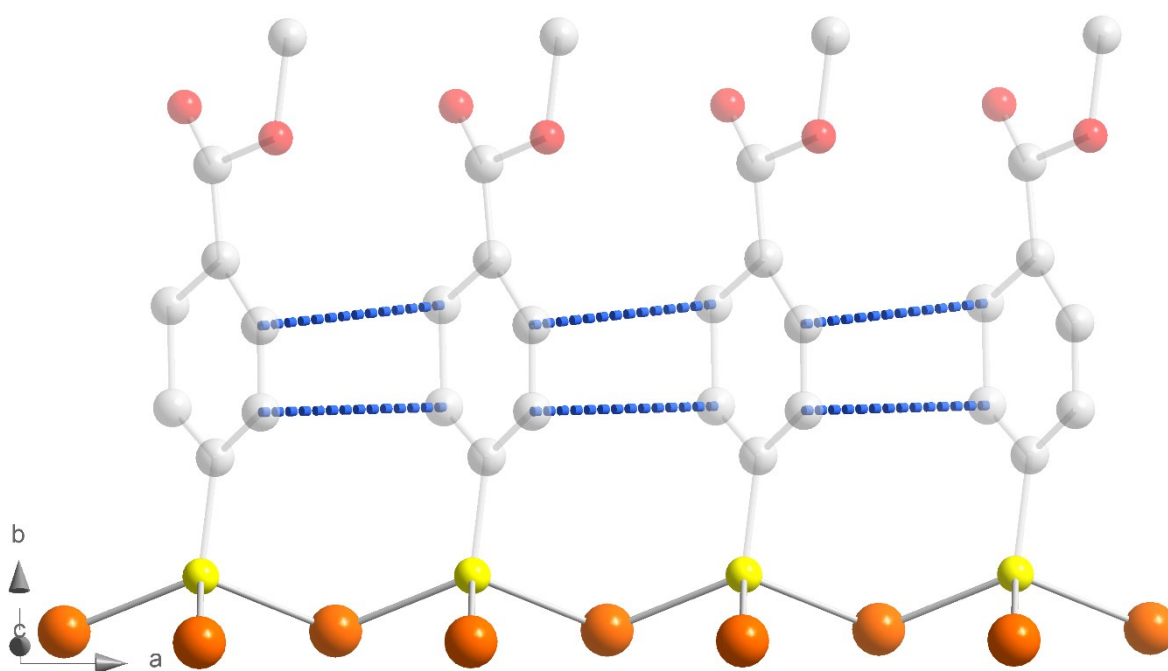


**Figure S2.** Representation of the parallel displaced  $\pi$ -stacked benzene rings in  $[\text{Cu}(p\text{-SPhCO}_2\text{Me})]_n$ . The C-C distances (dotted blue lines) are 3.458(2) and 3.479(1) Å.

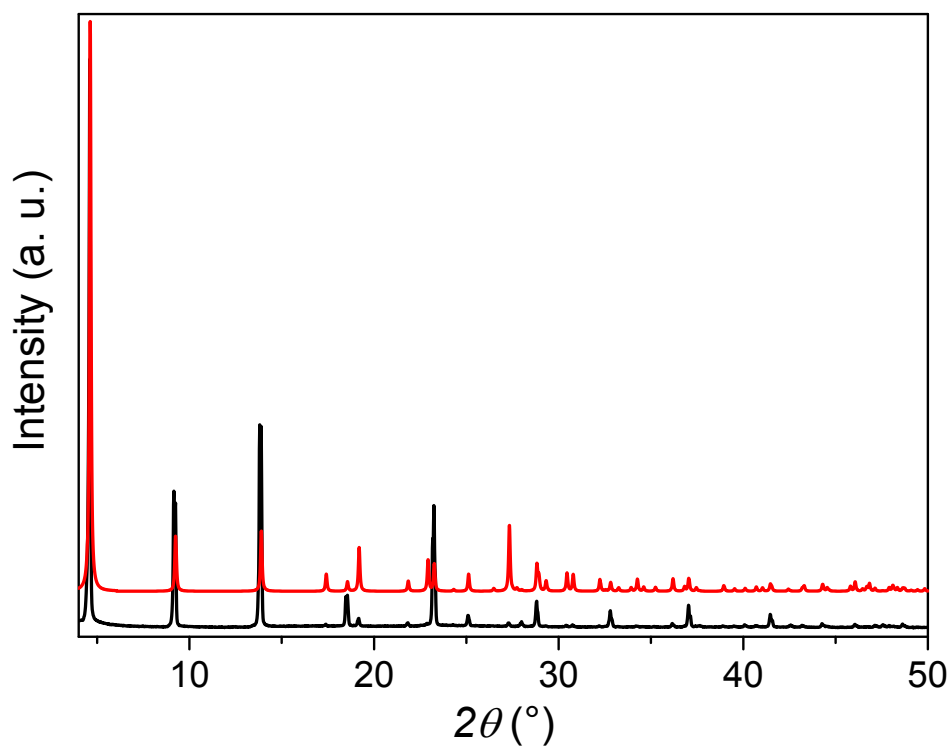


**Figure S3.** Experimental (black) and simulated (red) PXRD patterns of  $[\text{Cu}(p\text{-SPhCO}_2\text{Me})]_n$ .

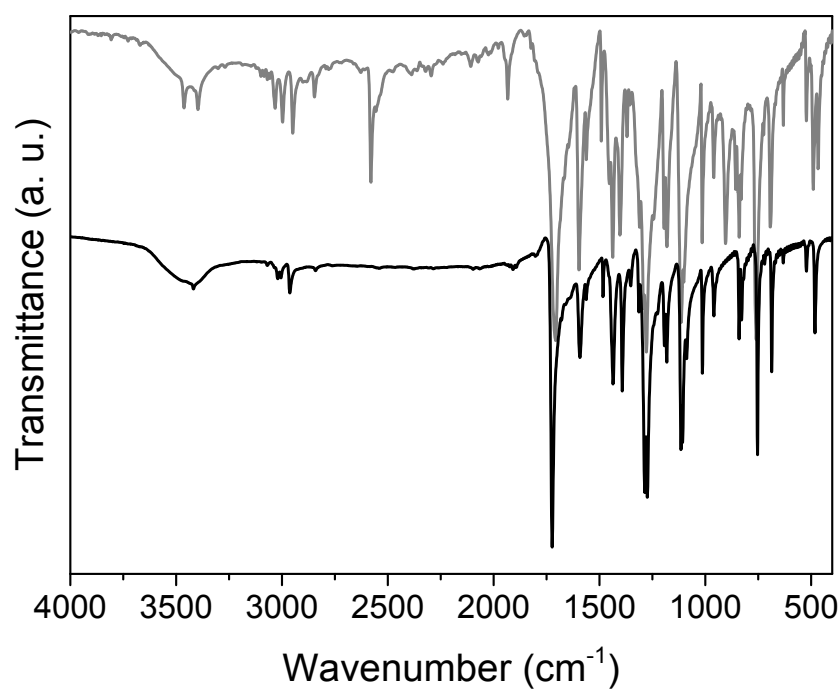


**Figure S4.** FT-IR spectra of  $p\text{-HSPhCO}_2\text{Me}$  (grey) and  $[\text{Cu}(p\text{-SPhCO}_2\text{Me})]_n$  (black). Antisymmetric vibrations of CO are present at  $1710$  and  $1724$   $\text{cm}^{-1}$  for  $p\text{-HSPhCO}_2\text{Me}$  and  $[\text{Cu}(p\text{-SPhCO}_2\text{Me})]_n$ , respectively.

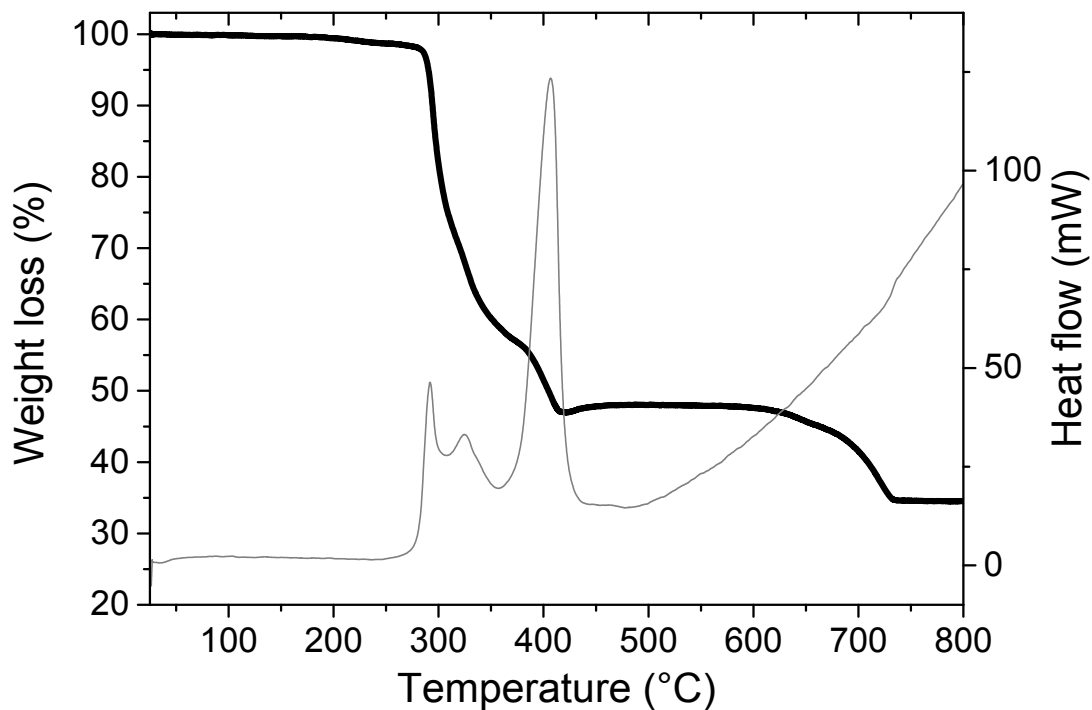


**Figure S5.** TGA (black) and DTA (grey) of  $[\text{Cu}(p\text{-SPhCO}_2\text{Me})]_n$  carried out under air at  $10^\circ\text{C}/\text{min}$ . The experimental value of remaining CuO is 34.5 % corresponding to the expected theoretical value (34.5 %).

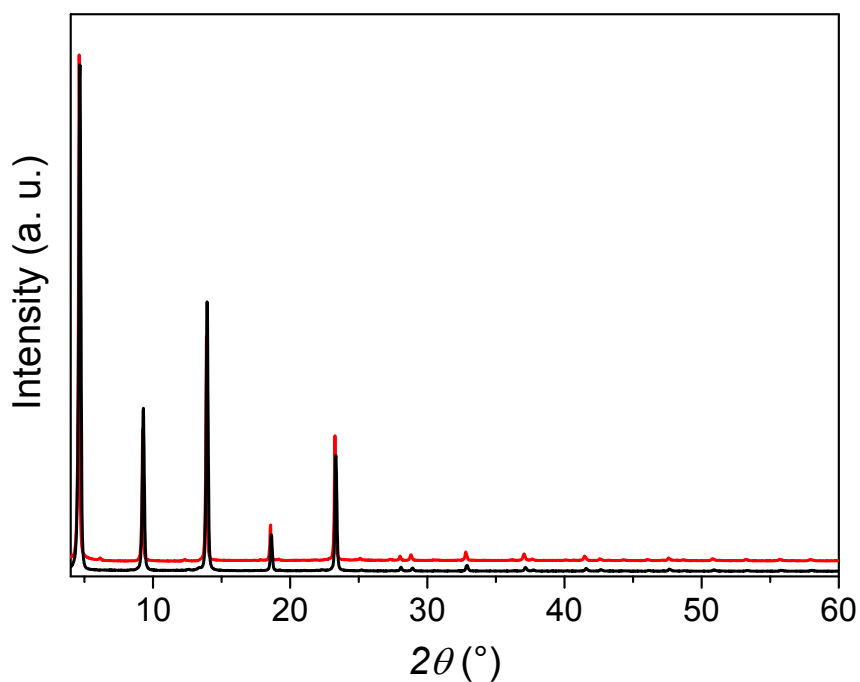


**Figure S6.** PXRD patterns of  $[\text{Cu}(p\text{-SPhCO}_2\text{Me})]_n$  before (black) and after (red) heating for 1 h at  $230^\circ\text{C}$  under air.

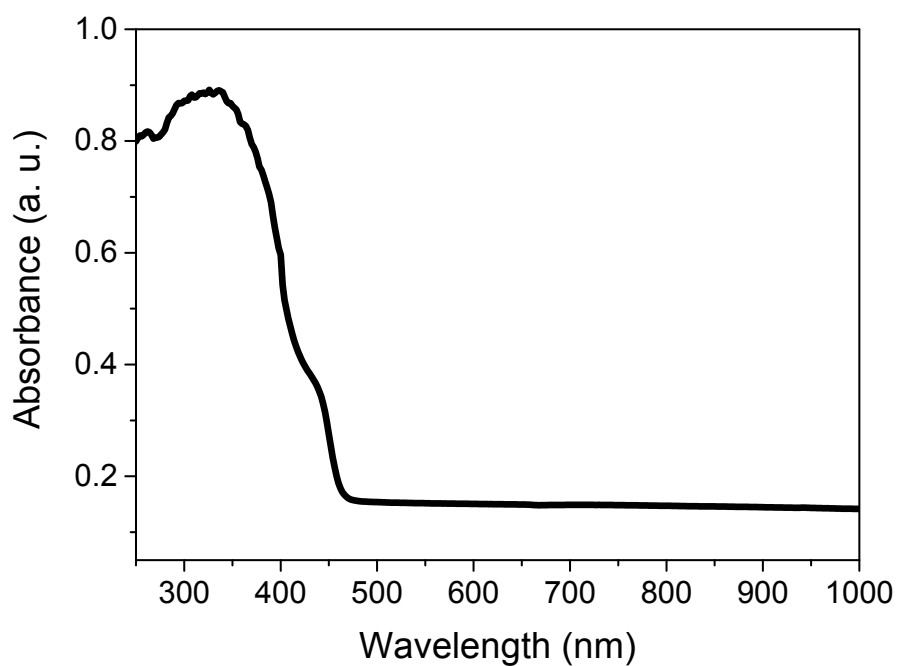


**Figure S7.** UV-vis absorption spectrum of  $[\text{Cu}(p\text{-SPhCO}_2\text{Me})]_n$  carried out in solid state at room temperature.

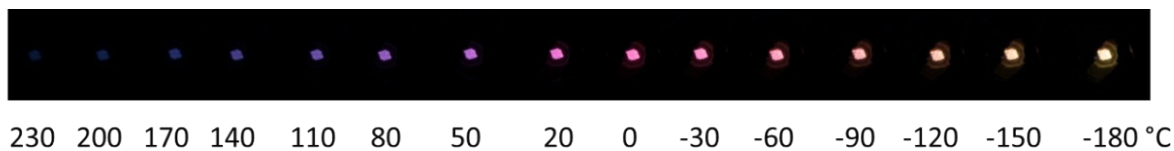


**Figure S8.** Photographies of  $[\text{Cu}(p\text{-SPhCO}_2\text{Me})]_n$  from 230 °C (left) to -180 °C (right) under UV light (365 nm).

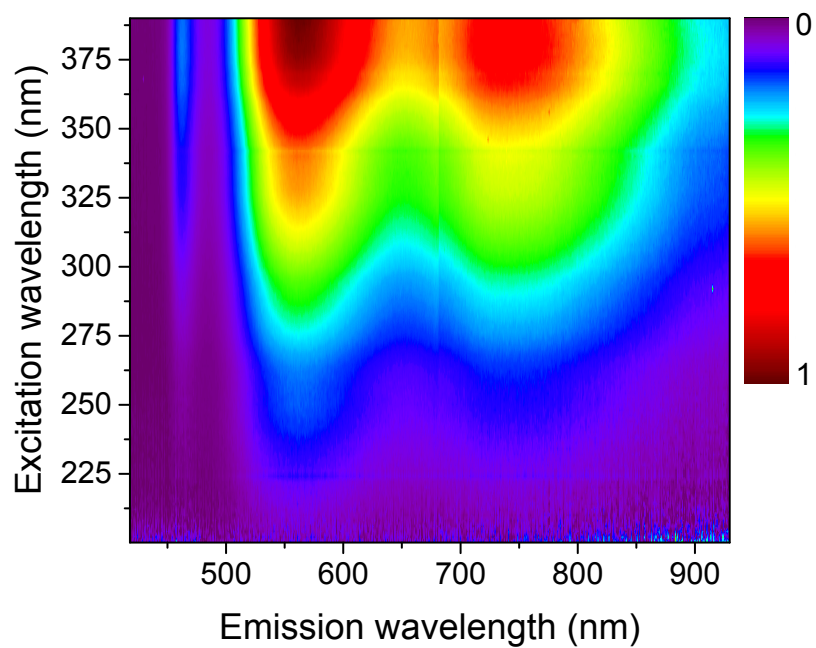


**Figure S9.** 2D map of the emission and excitation spectra of  $[\text{Cu}(p\text{-SPhCO}_2\text{Me})]_n$  carried out in solid-state at 93 K.

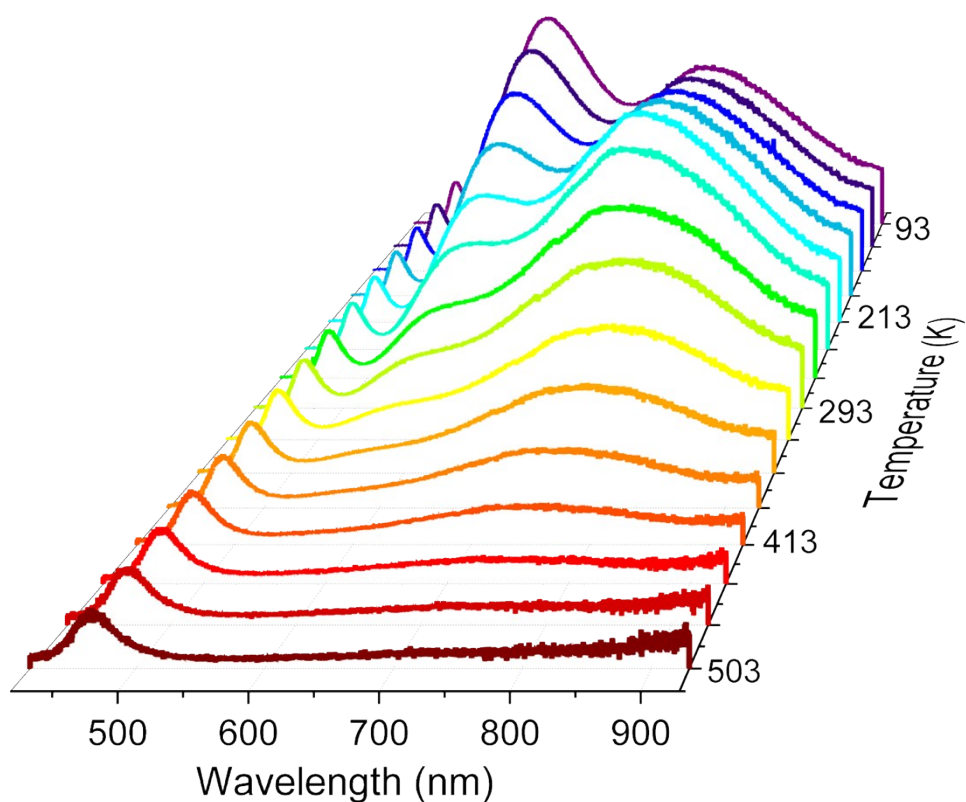


**Figure S10.** Emission spectra ( $\lambda_{\text{ex}} = 380 \text{ nm}$ ), normalized with the 460 nm peak intensities, of  $[\text{Cu}(p\text{-SPhCO}_2\text{Me})]_n$  carried out in solid-state with the temperature.

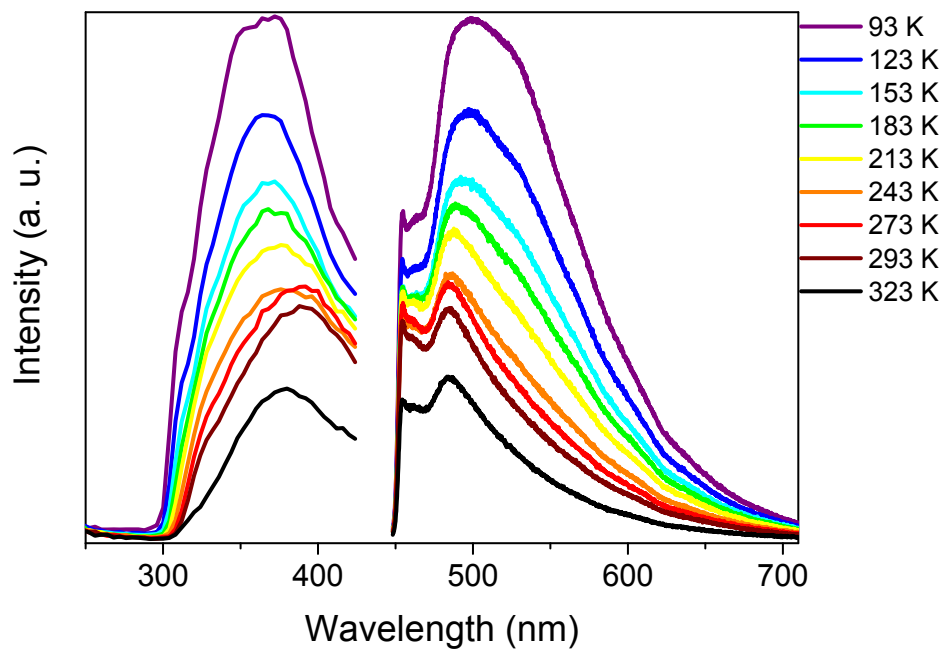


**Figure S11.** Excitation ( $\lambda_{em} = 498$  nm) and emission ( $\lambda_{ex} = 356$  nm) spectra of *p*-HSPHCO<sub>2</sub>Me carried out in solid-state with the temperature.

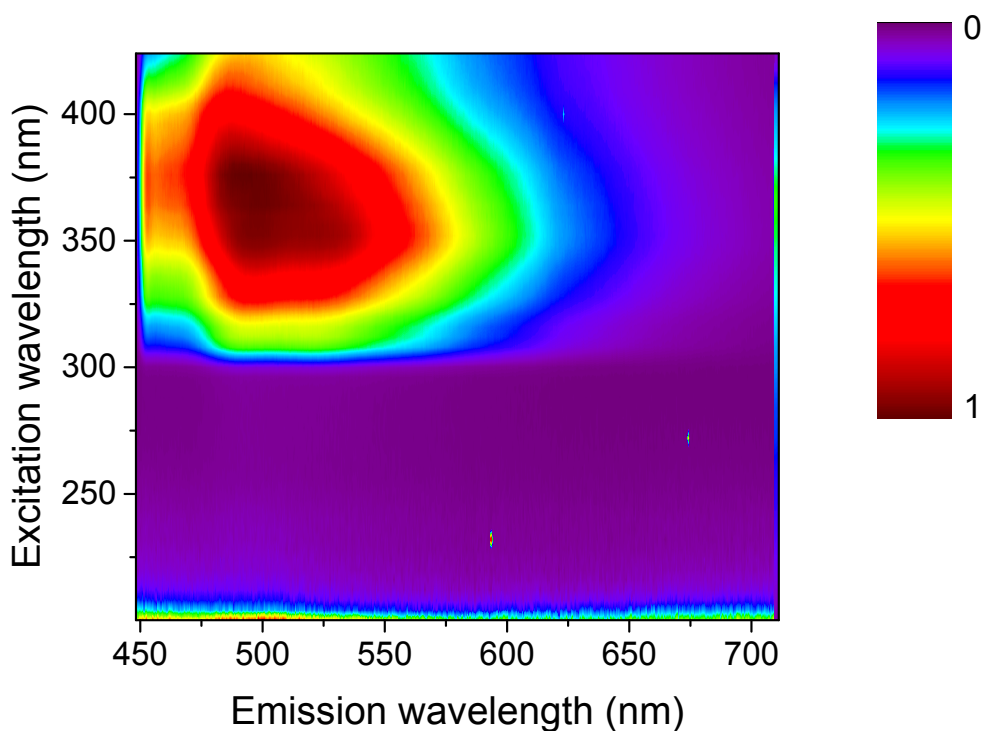


**Figure S12.** 2D map of the emission and excitation spectra of *p*-HSPHCO<sub>2</sub>Me carried out in solid-state at 93 K.

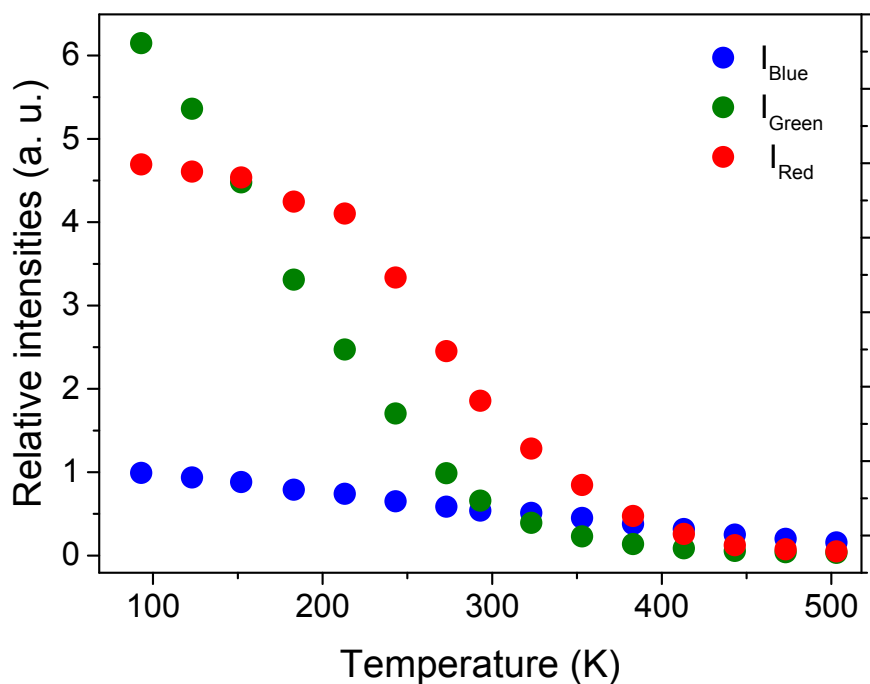


**Figure S13.** Plots of the emission intensities ( $\lambda_{\text{ex}} = 380 \text{ nm}$ ) of peaks centered at 462 nm ( $I_{\text{B}}$ ), 565 nm ( $I_{\text{G}}$ ) and 740 nm ( $I_{\text{R}}$ ). The intensities,  $I_{\text{B}}$  and  $I_{\text{G}}$ , are determined by the integration of the emission spectra between 452 and 472 nm, 555 and 575 nm and 730 and 750 nm, respectively.

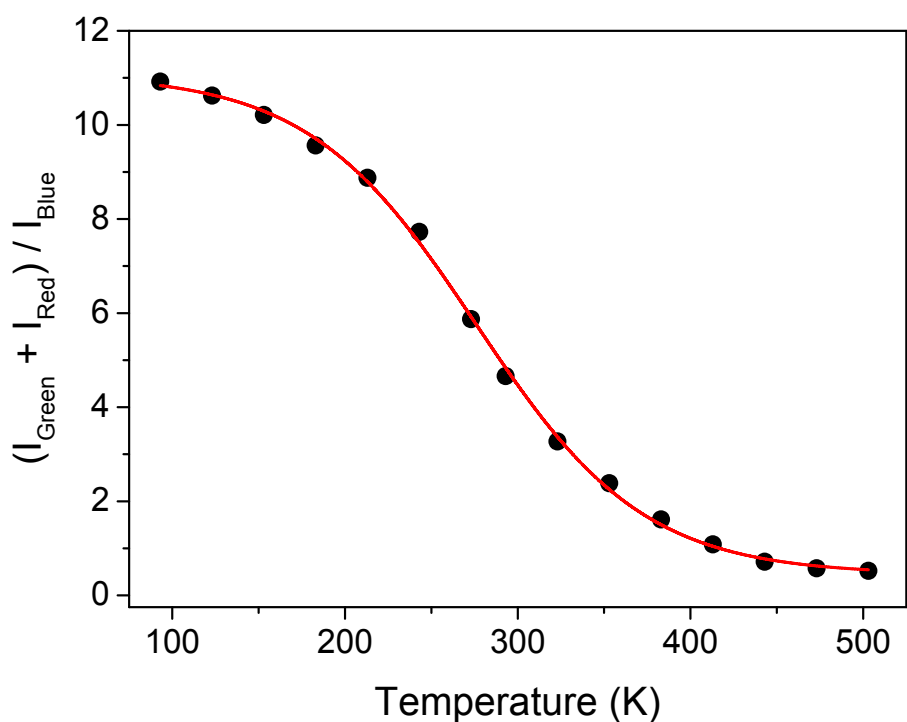


**Figure S14.** Plot of the  $(I_{\text{Green}} + I_{\text{Red}}) / I_{\text{Blue}}$  ratio with the temperature (black circles). The red line corresponds to the Boltzmann sigmoidal fit ( $R^2 = 0.999$ ) between 93 and 503 K.

$$\frac{(I_{Green} + I_{Red})}{I_{Blue}} = 0.44594 + \frac{10.63246}{1 + \exp\left(\frac{T - 275.9135}{48.59497}\right)}$$

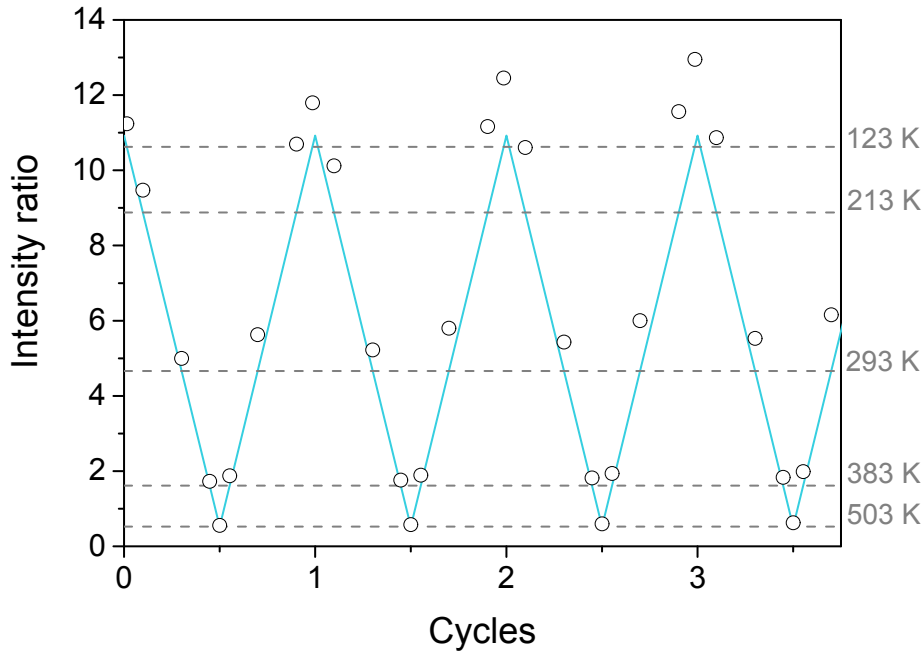


**Figure S15.** Intensity ratios obtained after few cycles of cooling and heating (black circles). The green lines are the calculated intensity ratios obtained from the first experiment (not shown).

To show how important change of parameters used for temperature sensing is both absolute and relative sensitivity are used. However, in order to have possibility to objectively compare the performances of the different luminescent thermometers, likewise thermometers that operate by different mechanisms or that are based on different material systems, the relative sensitivity ( $S_r$ ) is usually utilized and is defined as:

$$S_r = \frac{\partial P / \partial T}{P}$$

where  $P$  is the measured temperature-sensitive parameter, such as intensity, lifetime, wavelength or intensity ratio, and  $T$  is temperature.

**Table S3.** Comparison of sensitivities of other reported ratiometric luminescent MOF-based thermometers with  $[\text{Cu}(p\text{-SPhCO}_2\text{Me})]_n$ , including the origin of the dual emission, the fitting model, the working temperature range (K), the maximum relative sensitivity value ( $S_r$ , %  $\text{K}^{-1}$ ) and the temperature at which  $S_r$  is maximum ( $T_r$ , K).<sup>5</sup>

Luminescent MOF	Origin <sup>§</sup>	Fit <sup>¶</sup>	Temperature [K]	$S_r$ [% $\text{K}^{-1}$ ]	$T_r$ [K]
$[\text{Cu}(p\text{-SPhCO}_2\text{Me})]_n$	Intrinsic	Sig. Boltzmann	93-503	1.37	353
ZnATZ-BTB	Intrinsic	linear	30-130	5.29	30
Dycpia	Intrinsic	Boltzmann	298-473	0.42	473
$(\text{Me}_2\text{NH}_2)_3[\text{Eu}_3(\text{FDC})_4(\text{NO}_3)_4]$	Intrinsic	Sig. Boltzmann	12-320	2.7	170
$[\text{Eu}_{0.102}\text{Tb}_{0.898}(\text{notpH}_4)(\text{NO}_3)(\text{H}_2\text{O})]_2$	La dopping	Mott-Seitz	18-300	3.9	38
$\text{Eu}_{0.0069}\text{Tb}_{0.9931}\text{-DMBDC}$	La dopping	linear	50-200	1.15	200
$\text{Tb}_{0.9}\text{Eu}_{0.1}\text{PIA}$	La dopping	linear	100-300	3.27	300
$\text{Tb}_{0.50}\text{Eu}_{0.50}\text{PIA}$	La dopping	linear	75-275	2.02	275
$\text{Tb}_{0.98}\text{Eu}_{0.02}\text{-OA-DSTP}$	La dopping	linear	77-275	2.40	275
$\text{Tb}_{0.98}\text{Eu}_{0.02}\text{-BDC-DSTP}$	La dopping	linear	77-225	2.75	225
$\text{Tb}_{0.957}\text{Eu}_{0.043}\text{-cpda}$	La dopping	linear	40-300	16.0	300
$\text{Eu}_{0.7}\text{Tb}_{0.3}\text{-cam-Himdc}$	La dopping	linear	100-450	0.11	450
$\text{Eu}_{0.02}\text{Gd}_{0.98}\text{-DSB}$	La dopping	Arrhenius	20-300	4.75	20
$\text{Tb}_{0.99}\text{Eu}_{0.01}(\text{BDC})_{1.5}(\text{H}_2\text{O})_2$	La dopping	linear	290-320	0.31	318
$\text{Eu}_{0.0616}\text{Tb}_{0.9382}\text{pcdmb}$	La dopping	-	25-200	0.34	200
$\text{Eu}_{0.5}\text{Tb}_{0.5}\text{@In(OH)bpydc}$	La dopping	linear	283-333	2.53	333
ZJU-88 $\triangleright$ perylene	Orga dopping	linear	293-353	1.28	293
$\text{TbTATAB}\triangleright\text{C460}$	Orga dopping	linear	100-300	4.48	300

<sup>§</sup>La dopping : Lanthanide dopping ; Orga dopping: organic molecule dopping. <sup>¶</sup> Sig. Boltzmann : Sigmoidal Boltzmann

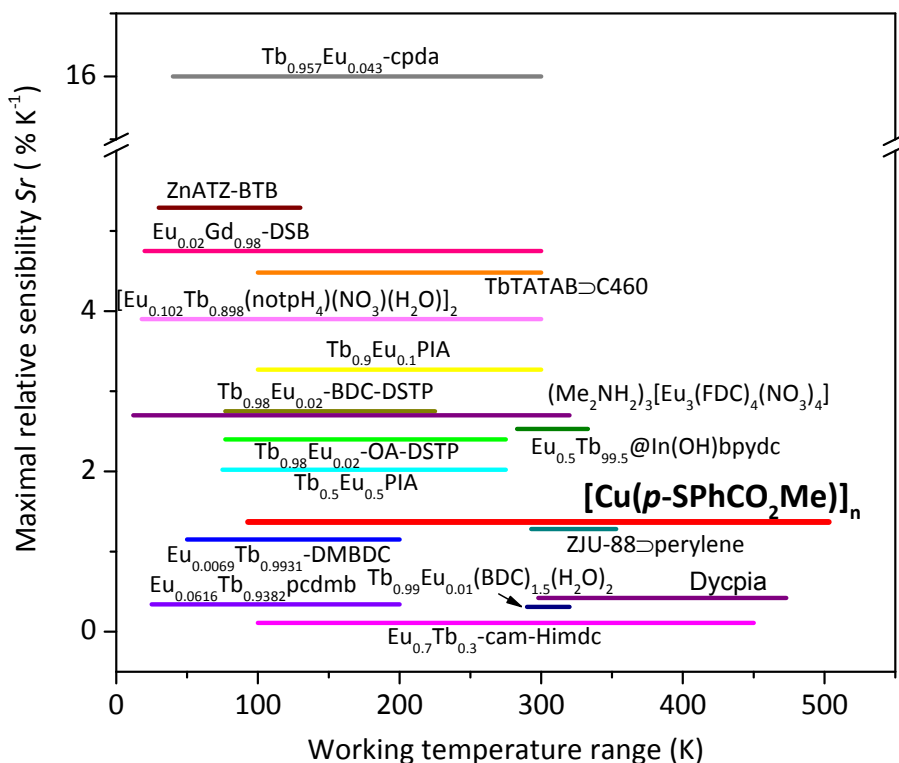


**Figure S16.** Visual comparison of the maximum relative sensitivity values ( $S_r$ , %  $K^{-1}$ ) with the working temperature ranges (K) of the reported ratiometric luminescent MOF-based thermometers with  $[Cu(p\text{-SPhCO}_2\text{Me})]_n$ .<sup>5</sup>

- [1]. *CrysAlisPRO*, 1.171.38.43 Rigaku OD, **2015**.
- [2]. R. C. Clark; J. S. Reid, *Acta Cryst., Sect. A*, **1995**, *51*, 887.
- [3]. A. Altomare; M. C. Burla; M. Camalli; G. L. Casciarano; C. Giacovazzo; A. Guagliardi; A. Grazia; G. Moliterni; G. Polidori; R. Spagna, *J. Appl. Cryst.*, **1999**, *32*, 115.
- [4]. P. W. Betteridge; J. R. Carruthers; R. I. Cooper; K. Prout; D. J. Watkin, *J. Appl. Cryst.*, **2003**, *36*, 1487.
- [5]. (a) R. F. D'Vries; S. Alvarez-Garcia; N. Snejkó; L. E. Bausa; E. Gutierrez-Puebla; A. de Andres; M. A. Monge, *J. Mater Chem. C*, **2013**, *1*, 6316; (b) Y. Cui; F. Zhu; B. Chen; G. Qian, *Chem. Commun.*, **2015**, *51*, 7420; (c) M. Ren; C. D. S. Brites; S.-S. Bao; R. A. S. Ferreira; L.-M. Zheng; L. D. Carlos, *J. Mater Chem. C*, **2015**, *3*, 8480; (d) L. Li; Y. Zhu; X. Zhou; C. D. S. Brites; D. Ananias; Z. Lin; F. A. Almedia Paz; J. Rocha; W. Huang; L. D. Carlos, *Adv. Funct. Mater.*, **2016**, *26*, 8677; (e) T. Xia; T. Song; Y. Cui; Y. Yang; G. Qian, *Dalton Trans.*, **2016**, *45*, 18689; (f) H. Zhang; C. Lin; T. Sheng; S. Hu; C. Zhuo; R. Fu; Y. Wen; H. Li; S. Su; X. Wu, *Chem. Eur. J.*, **2016**, *22*, 4460; (g) T. Xia; Y. Cui; Y. Yang; G. Qian, *J. Mater Chem. C*, **2017**, *5*, 5044.